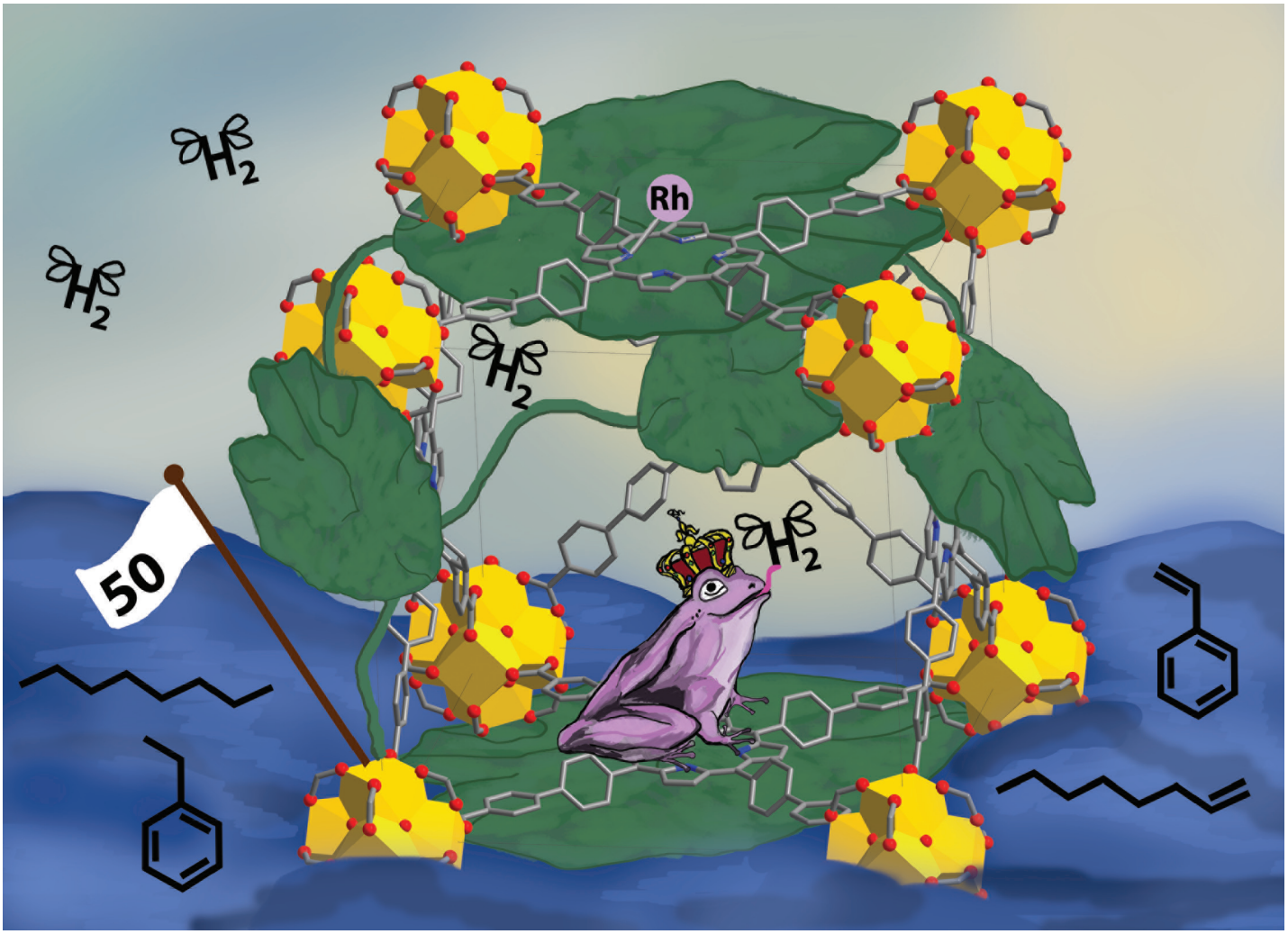

Showcasing research from Doctor Bury's MOF laboratory, Faculty of Chemistry, University of Wrocław, Poland.

Immobilization of Rh(I) precursor in a porphyrin metal–organic framework – turning on the catalytic activity

Porphyrin metal-organic frameworks were used for the incorporation of Rh(I) species by a postsynthetic metallation under mild conditions. New phosphine-free heterogeneous catalysts, active in the hydrogenation of unsaturated hydrocarbons under mild reaction conditions (30 °C and 1 atm H_2), were obtained. This simple postsynthetic modification approach presents new possibilities for utilization of Rh-based catalytic systems with porphyrin MOFs as supports.

As featured in:

See Wojciech Bury *et al.*, *Dalton Trans.*, 2021, **50**, 9051.

ROYAL SOCIETY OF CHEMISTRY

rsc.li/dalton

Registered charity number: 207890

Dalton Transactions

ROYAL SOCIETY OF CHEMISTRY

PAPER

View Article Online
View Journal | View Issue

Cite this: *Dalton Trans.*, 2021, **50**, 9051

Immobilization of Rh(I) precursor in a porphyrin metal–organic framework – turning on the catalytic activity†

Anna M. Szczepkowska, [a] Mateusz Janeta, [a] Miłosz Siczek, [a] Włodzimierz Tylus,[b] Anna M. Trzeciak[a] and Wojciech Bury *[a]

Received 16th February 2021,
Accepted 4th May 2021

DOI: 10.1039/d1dt00518a

rsc.li/dalton

Two model porphyrin metal–organic frameworks were used for the incorporation of Rh(I) species by a post-synthetic metallation under mild conditions. As a result, new rhodium MOFs (Rh/MOFs), **Rh/PCN-222** and **Rh/NU-1102**, were synthesized and structurally characterized. To illustrate the potential of this catalytic platform, we use Rh/MOFs as phosphine-free heterogeneous catalysts in the hydrogenation of unsaturated hydrocarbons under mild reaction conditions (30 °C and 1 atm H_2). We found that for our Rh/MOFs an activation step is required during the first run of the catalytic process. The presence of Rh–CO moieties allowed us to monitor the activation pathway of the catalyst under a H_2 atmosphere, by *in situ* Diffuse Reflectance Infrared Fourier Transform Spectroscopy (DRIFTS). After activation, the catalyst remains highly active during the subsequent catalytic cycles. This simple post-synthetic modification approach presents new possibilities for the utilization of Rh-based catalytic systems with robust porphyrin-based MOFs as supports.

Introduction

Soluble rhodium complexes have found many applications in laboratory and industrial processes. The most prominent examples include alkene hydrogenation,[1–4] alkene hydroformylation,[5–7] and methanol carbonylation.[8–10] Due to the high price of noble metals, especially rhodium, and for better recovery and recyclability of the catalyst, construction of supports for molecular complexes is of great importance.[11] In this view, Metal–Organic Frameworks (MOFs) offer well-defined and stable environments for the incorporation of various molecular entities, including molecular catalysts. To date, many approaches for incorporating catalytically active centers into different MOFs have been demonstrated,[12,13] including covalent attachment of the metal centres to the nodes, linkers or as charge-balancing guests counterions inside the pores (Fig. 1). For the hydrogenation of olefins, several strategies of MOF-based catalysts have been devised,[14] including coordinatively unsaturated metal sites,[15–17] noble-metal nanoparticles encapsulated inside MOF crystallites,[18–20] hollow spheres,[21] and core–shell systems.[22] In this context, the incorporation of rhodium into a porous framework, as a structure-determining component, remains challenging despite the rich molecular coordination chemistry of this noble metal. The Rh_2-paddlewheel cluster is an archetypal motif for the direct construction of MOFs with Rh(II) centers (Fig. 1, **I**); however, these systems are very rare, due to synthetic difficulties and low stability.[23] More often, other pathways of rhodium incorporation have been involved, which rely on the modifications of more robust and stable host frameworks. Depending on the desired catalytic function, the reactive species can be introduced post-synthetically, by node modification (Fig. 1, **II**),[24] ion exchange (**III**),[25,26] post-synthetic metalation (**IV**),[27,28] linker exchange (**V**),[29] or metal exchange in a metallolinker (**VI**).[30] Usually, rhodium-based catalysts contain phosphines as supporting ligands. To avoid highly toxic ligands, it is of importance to find more environmentally friendly alternatives. The limited number of studies involving the application of porphyrins as supporting ligands in rhodium-based catalytic processes turned our attention to this group of building blocks.[31] Rhodium porphyrin complexes have been actively investigated for over 50 years,[32] leading to important discoveries, including catalytic enantioselective cyclopropanation[33,34] and selective C–H and C–C activation.[35,36] The utilization of porphyrin macrocycle as a supporting ligand allows access to various valence states of Rh (*e.g.* +I, +II and +III).[32] Particularly interesting is the activation

[a]*Faculty of Chemistry, University of Wrocław, F. Joliot-Curie 14, 50-383 Wrocław, Poland. E-mail: wojciech.bury@chem.uni.wroc.pl*

[b]*Department of Advanced Material Technologies, Faculty of Chemistry, Wrocław University of Science and Technology, Wybrzeże Wyspiańskiego 27, 50-370 Wrocław, Poland*

† Electronic supplementary information (ESI) available. CCDC 2051075–2051077. For ESI and crystallographic data in CIF or other electronic format see DOI: 10.1039/d1dt00518a

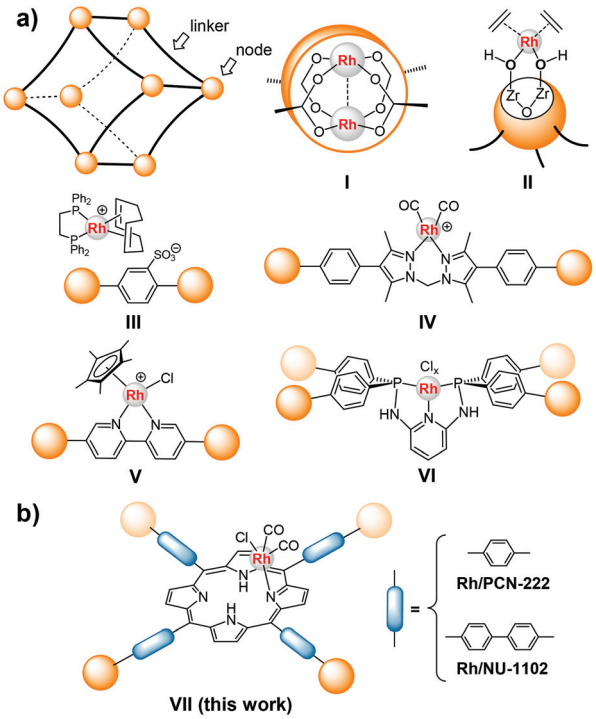

Fig. 1 (a) Structural motifs for the incorporation of Rh molecular catalytic systems supported by various MOFs, and (b) the coordination mode of rhodium in the Rh/MOFs presented in this work.

of molecular hydrogen by rhodium complexes,[37–40] including Rh/porphyrin systems as promising candidates.[41–45]

The spatial separation of metallolinkers inside the porous structure is crucial when the active catalytic centers are generated, for example in tandem catalytic systems.[46] In this regard, porphyrin-based MOFs combine all the required features of a heterogeneous catalyst, *i.e.* an efficient platform for the metallic centers within the rigid 3D porous structure.

Insertion of rhodium into the porphyrin core can be achieved by direct metallation, which is usually carried out with a free base porphyrin and a rhodium salt in a high boiling solvent, to afford the corresponding rhodium(III) porphyrin halide. Lower oxidation states of rhodium tend to undergo transformation to higher valence states by oxidative addition, therefore *de novo* synthesis of porphyrin-based MOFs with Rh(I) has not been reported to date. Recently, Bloch *et al.* demonstrated a single crystal study of the catalytic carbonylation of CH_3I on a Mn(II)-based MOF, in which the chelating linker, containing the (3,5-dimethylpyrazolyl)methane moiety, was metallated with the $[Rh(CO)_2Cl]_2$ precursor.[27,28]

Herein, we report a facile synthesis and catalytic activity of the new phosphine-free rhodium MOFs (Rh/MOFs), **Rh/PCN-222** and **Rh/NU-1102** (Fig. 1, **VII**), by a one-step post-synthetic modification of the Zr-based parent frameworks, **PCN-222** and **NU-1102**, under mild reaction conditions. The rhodium(I) centers were introduced into the organic linkers using $[Rh(CO)_2Cl]_2$ as a precursor (Fig. 2). We probed these new Rh/MOFs as catalysts in the hydrogenation of unsaturated hydrocarbons at room temperature and 1 atm of H_2, and the results show high activity of Rh/MOFs in these reactions. The activation pathway of Rh/MOFs was studied by *in situ* solid-state Diffuse Reflectance Infrared Fourier Transform Spectroscopy (DRIFTS), which showed that the activation of Rh centers proceeds by the reaction of CO ligands with H_2 leading to formate, formic acid or methanol as by-products. After activation, the catalytic platform remains active in several consecutive catalytic cycles.

Experimental

Preparation of organic linkers

meso-Tetrakis[4-(methoxycarbonyl)phenyl]porphyrin (H_2TMCPP, **1a**), *meso*-tetrakis-(4-methylcarboxybiphenyl)porphyrin

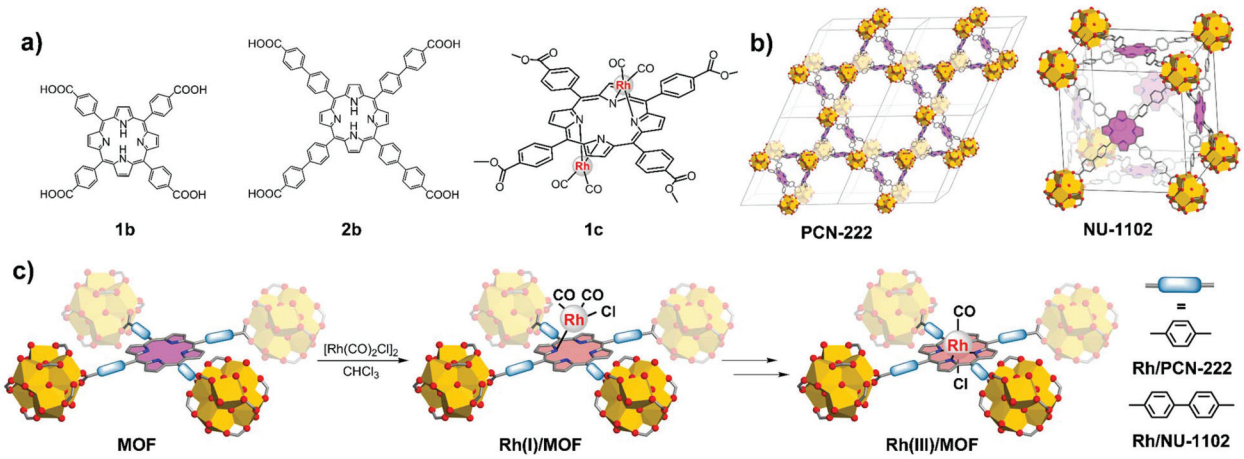

Fig. 2 (a) Schematic representation of the prolinkers **1b** and **2b**, and the molecular reference compound **1c**; (b) crystal networks of **PCN-222** and **NU-1102**; and (c) schematic representation of the post-synthetic metalation of **PCN-222** or **NU-1102**, leading to **Rh(I)/MOF** and **Rh(III)/MOF** ("aging" process).

(H_2TMCBPP, **2a**), *meso*-tetrakis(4-carboxyphenyl)porphyrin (H_2TCPP, **1b**), *meso*-tetrakis-(4-carboxybiphenyl)porphyrin (H_2TCBPP, **2b**), **PCN-222** and **NU-1102** were prepared according to the previously reported procedures.[47,48]

Synthesis of (TMCPP)$Rh_2(CO)_4$ (1c)

The synthesis was adapted from the literature procedure for a similar compound.[49] To a Schlenk flask charged with **1a** (0.050 g, 0.06 mmol) and anhydrous sodium acetate (0.172 g, 2.10 mmol) $CHCl_3$ (10 mL) and a solution of $[Rh(CO)_2Cl]_2$ (34 mg, 0.09 mmol) in $CHCl_3$ (4 mL) were added under a N_2 atmosphere. Then the reaction was carried out with vigorous stirring at 25 °C for 2.5 h. The resulting mixture was washed with water, dried with $MgSO_4$ and evaporated. The residue was chromatographed on silica gel with $CHCl_3$ and the mixture $CHCl_3$: CH_3OH (100 : 1). Crystals were collected by recrystallization from $CHCl_3$ (0.060 g, 0.053 mmol, 90.2% yield).

Synthesis of Rh/PCN-222

A microwave reaction glass vial (Biotage, 5–10 mL) was charged with approximately 0.5 g of solvated crystalline material **PCN-222** and 1 mL of CH_2Cl_2 under a N_2 atmosphere. Then a solution of 25 mg of $[Rh(CO)_2Cl]_2$ in CH_2Cl_2 (4 mL) was added, and the vial was placed in an Eppendorf ThermoMixer (550 rpm) at 60 °C for 24 h. The resulting modified crystals were washed by adding fresh CH_2Cl_2 (5 mL) and leaving the vial in the ThermoMixer (550 rpm) for 0.5 h at 60 °C. The washing procedure was repeated until the solvent over the crystals became colorless (5 times). The solvent was decanted and the purple crystals were dried in an oven at 60 °C for 24 h.

Synthesis of Rh/NU-1102

A microwave reaction glass vial (Biotage, 5–10 mL) was charged with approximately 1.0 g of solvated crystalline material **NU-1102** with 1 mL of CH_2Cl_2 under a N_2 atmosphere. Then a solution of 35 mg of $[Rh(CO)_2Cl]_2$ in CH_2Cl_2 (4 mL) was added, and the vial was placed in an Eppendorf ThermoMixer (550 rpm) at 60 °C for 24 h. The resulting modified crystals were washed by adding fresh CH_2Cl_2 (5 mL) and leaving the vial in the ThermoMixer (550 rpm) for 0.5 h at 60 °C. The washing procedure was repeated until the solvent over the crystals became colorless. The solvent was decanted and the purple crystals were dried in an oven at 60 °C for 24 h.

General procedure for the hydrogenation of olefins

To a Schlenk flask with 4 mg of the corresponding Rh/MOF (0.3 mg, 1 mol% Rh) under a N_2 atmosphere, a dry solvent (4 mL) and the selected unsaturated hydrocarbon were added (0.3 mmol). Next, the gas phase was removed by short evacuation from the Schlenk flask and H_2 was introduced and left under 1 atm of H_2 using a balloon. The resulting mixture was stirred at 30 °C for a limited time under the H_2 atmosphere (1 atm). After this time, 0.1 mL of solution was collected above the crystals of Rh/MOF, filtered with cotton wool, diluted with 0.5 ml of CH_2Cl_2 and analyzed by using a GC-flame ionization detector.

Results and discussion

Synthesis and structural characterization of Rh/MOFs

In our approach, we decided to explore the catalytic properties of porphyrin-based Rh(I) complexes embedded inside a robust MOF. It has been shown previously that rhodium(I) can form bimetallic complexes [(por)M_2L_4] (M = metal; L = ligand) involving classical or *N*-confused porphyrins.[32,50,51] This type of coordination mode has been rarely observed for transition metals; however, for rhodium(I), several complexes of this type have been described, with the emphasis on their synthetic and catalytic potential.[52,53] Two possible reaction pathways can be regarded when the $[Rh(CO)_2Cl]_2$ precursor is used in the synthesis of new complexes, by forming monomeric $[Rh(CO)_2Cl]$ species or by disproportionation, yielding the square-planar cationic $[Rh(CO)_2]^+$ and anionic $[Rh(CO)_2Cl_2]^-$ species.[54,55] For a better understanding of the metalation process in the porphyrin-based MOF, we prepared a molecular reference **1c**, where $[Rh(CO)_2]^+$ is stabilized by the porphyrin ligand. To obtain **1c**, the reaction of **1a** with $[Rh(CO)_2Cl]_2$ was carried out in chloroform with sodium acetate as a base. The crystals of **1c** were obtained by slow evaporation of the solvent and were analyzed by single-crystal X-ray diffraction. The molecular structure of **1c** is shown in Fig. S26.† In the structure of **1c**, the Rh (I) centers are placed outside the porphyrin plane, and to each rhodium atom two carbonyl ligands are attached, completing the square-planar geometry of the metal.

In our study, we employed two tetratopic linkers with different spacer lengths: H_2TCPP (**1b**) and H_2TCBPP (**2b**). Compounds **1b** and **2b** were used to construct well-characterized three-dimensional frameworks **PCN-222** ($Zr_6O_4(OH)_4(BA)_4L_2$, L = H_2TCPP^{4-} and BA = $PhCOO^-$) and **NU-1102** ($Zr_6O_4(OH)_4L'_3$, L′ = H_2TCBPP^{4-}), with different pore sizes and network topologies – *csq* and *ftw*, respectively. The post-synthetic metalation was carried out using $[Rh(CO)_2Cl]_2$ as the metal source. A sample of each MOF was soaked in a degassed solution of $[Rh(CO)_2Cl]_2$ in CH_2Cl_2 in a sealed vial. The efficiency of metalation of **PCN-222** and **NU-1102** was monitored by the ICP analysis. After 24 h of the reaction at 60 °C, the composition of the metalated MOFs was established and the following formulas were derived: for **Rh/PCN-222** – $Rh_{2.4}Cl_{2.4}Zr_6O_4(OH)_4(BA)_4L_2$, and for **Rh/NU-1102** – $Rh_{3.4}Cl_{4.6}Zr_6O_4(OH)_4L_3$, suggesting that, in contrast to **1c**, the rhodium to linker ratio was approximately 1 : 1. The crystallinity of the resulting Rh/MOFs was confirmed by the PXRD studies (Fig. 3a and b). Comparing the powder diffraction patterns before and after metalation, it was noticed that the network topology of the Rh/MOFs was preserved. The morphology and distribution of the elements in the resulting materials were further investigated by scanning electron microscopy (SEM) and Energy Dispersive Spectroscopy (EDS) (Fig. 3c and d). From the SEM images, we conclude that the crystallites of **Rh/PCN-222** and **Rh/NU-1102** retained the shape and size of the parent crystals. Additionally, the EDS mapping of the elements on the crystallites showed an even distribution of Zr and Rh over the entire crystal (Fig. 3c and d), and the Rh/

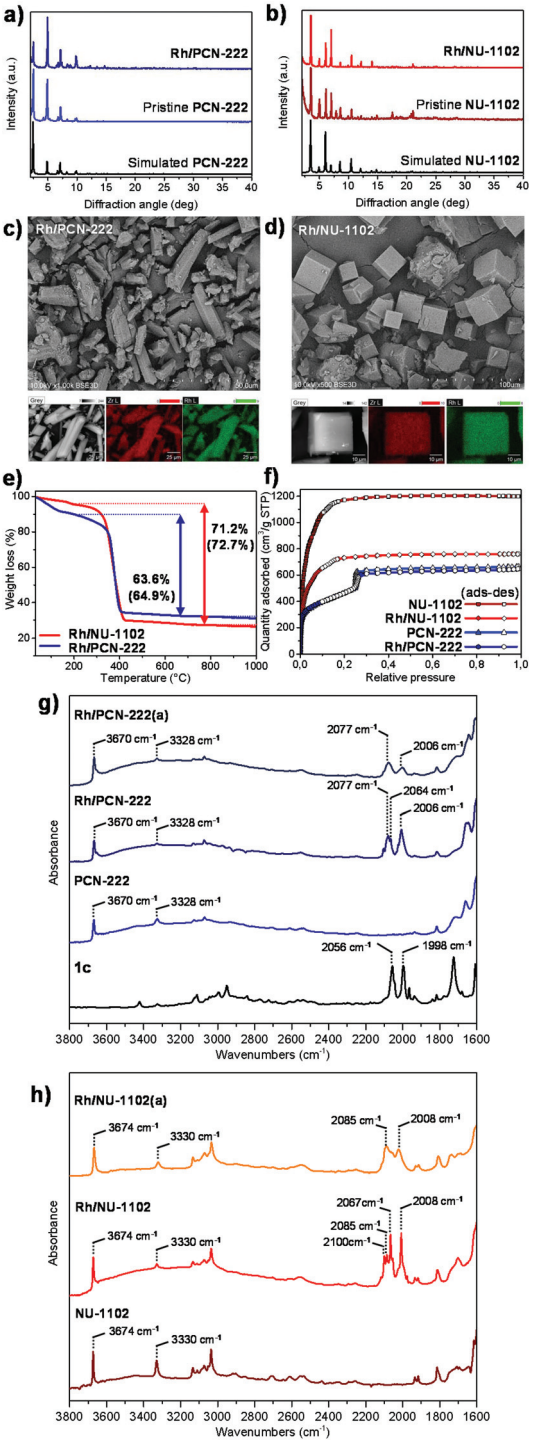

Fig. 3 Simulated and experimental PXRD patterns of: (a) **Rh/PCN-222** and (b) **Rh/NU-1102**; SEM micrographs and EDS mapping analysis for: (c) **Rh/PCN-222** and (d) **Rh/NU-1102**; (e) TGA profiles of Rh/MOFs; (f) comparison of the experimental N_2 isotherms of **NU-1102**, **Rh/NU-1102**, **PCN-222** and **Rh/PCN-222** obtained at 77 K; and comparison of the DRIFTS spectra for: (g) **Rh/PCN-222** and (h) **Rh/NU-1102**.

Zr ratio was maintained in the cross-sections of the crystals (see the ESI, section S4.1†). Moreover, based on the EDS analysis, the presence of chlorine was observed (the Rh : Cl ratio of ~1 : 1), which suggests the coordination of the Cl^- ligand to the rhodium atom, as shown in Fig. 2c. To gain more insights into the coordination environment of the rhodium centers, the solid-state DRIFTS measurements were carried out. The DRIFTS spectra for the Rh/MOFs show two strong bands of carbonyl vibrations at 2064 cm^{-1} and 2006 cm^{-1} for **Rh/PCN-222**, and similarly at 2067 cm^{-1} and 2008 cm^{-1} for **Rh/NU-1102** (Fig. 3g and h). These results suggest the presence of two possible types of Rh–CO moieties in the Rh/MOFs, as shown in Fig. 2c. Additionally, for **Rh/PCN-222**, a broad signal at 2077 cm^{-1} was observed, indicating the presence of another type of CO ligand bound to the rhodium center. This vibration indicates the coexistence of the [Rh(III)(Por)(CO)(Cl)] moiety,[56] which was also confirmed by the single-crystal X-Ray analysis, suggesting the occurrence of an "aging" process in the crystals. Moreover, in the region of N–H vibrations, a strong peak at 3328 cm^{-1} is present, indicating the presence of a free-base porphyrin. For comparison, the DRIFTS absorbance spectrum was also acquired for a solid sample of **1c**, which we used as a well-defined reference compound. In the spectrum of **1c**, only two strong carbonyl vibrations at 2056 cm^{-1} and 1998 cm^{-1} are present, resulting from the vibrations of two carbonyl ligands at the Rh center in **1c** (Fig. 3g), which supports the proposed coordination environment of the rhodium center in the Rh/MOFs.

The XPS study was conducted to gain information about the elemental compostion of Rh/MOFs and chemical states of Rh and Zr centers before and after the catalytic reaction for the studied Rh/MOFs. Unfortunately, the binding energies of Rh (0), Rh(I), Rh(II) and Rh(III) available in the literature overlap (see the ESI, section S4.2†).[57–59] To determine the degree of Rh oxidation in the **Rh/PCN-222** catalyst, the XPS spectrum of 1c was used as a reference for Rh(I). For **1c**, two intense, symmetric peaks for Rh 3d5/2 and Rh 3d3/2 were observed with the binding energies of 309.2 and 313.8 eV, respectively. Similarly, for **Rh/PCN-222**, we observed two symmetric peaks at 309.6 and 314.3 eV, which are in good agreement with the energies obtained for **1c**, suggesting a similar coordination environment and valency of the rhodium centers.

The single crystal X-ray diffraction performed on the crystals of **Rh/PCN-222(a)** and **Rh/NU-1102(a)** (aged samples) confirmed the metalation of the porphyrin macrocycle.[60] The structural models suggest oxidative transformation of the initially formed **Rh(I)/MOF** into their corresponding **Rh(III)/MOF** (Fig. 2c and section S4.4 in the ESI†), with only one CO and one Cl^- ligand bound to the Rh atom.

To gain some insights into the thermal stability and decomposition pathway of **Rh/PCN-222** and **Rh/NU-1102**, thermogravimetric analysis (TGA) was performed under an oxidative atmosphere of synthetic air (O_2 : N_2 = 20 : 80). For both MOFs, a small weight loss can be observed below 100 °C, associated with the removal of the guest solvent molecules. Both materials exhibit significant thermal stability up to 380 °C (Fig. 3e). The obtained ceramic yields at 800 °C are in good agreement with the theoretical values, for **Rh/PCN-222**

and **Rh/NU-1102** – 63.6 wt% (theor.: 64.9 wt%) and 71.2 wt% (theor.: 72.7 wt%), respectively.[61] In addition, the thermal stability of Rh–CO moieties was further examined by Variable-Temperature DRIFTS (VT-DRIFTS) in the range of 30–300 °C, which demonstrated a gradual disappearance of carbonyl bands above 160 °C (see the ESI, section S4.5†).

The porosity of **Rh/PCN-222** and **Rh/NU-1102** was examined by N_2 adsorption experiments at 77 K. Permanent porosity of both materials was confirmed based on the dinitrogen adsorption, as shown in Fig. 3h. The calculation of Brunauer–Emmett–Teller surface area (S_{BET}) for **Rh/PCN-222** and **Rh/NU-1102** resulted in values of 1657 and 2915 $m^2\ g^{-1}$, respectively, confirming remarkably high porosity of the obtained Rh/MOFs (Fig. 3f).

Table 1 Catalytic activity of Rh/MOFs in the hydrogenation of different unsaturated hydrocarbons

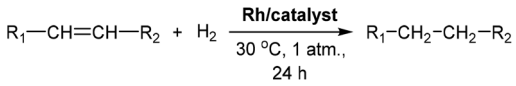

Entry	Catalyst[a]	Alkene	Solvent	Yield (%)
1	**1c**	1-Octene	Toluene	46
2	**1c**	1-Octene	CH_2Cl_2	11
3	**1c**	Styrene	Toluene	14
4	**1c**	Styrene	CH_2Cl_2	1
5	**PCN-222**	1-Octene	Toluene	0
6	**Rh/PCN-222**	1-Octene	Toluene	99/65[b]
7	**Rh/PCN-222**	1-Octene	CH_2Cl_2	99
8	**Rh/PCN-222**	Styrene	Toluene	99
9	**Rh/PCN-222**	Styrene	CH_2Cl_2	95
10	**Rh/PCN-222**	Cyclohexene	Toluene	99
11	**Rh/PCN-222**	2-Cyclohexen-1-one	Toluene	99
12	**NU-1102**	1-Octene	Toluene	0
13	**Rh/NU-1102**	1-Octene	Toluene	99
14	**Rh/NU-1102**	1-Octene	CH_2Cl_2	83
15	**Rh/NU-1102**	Styrene	Toluene	99
16	**Rh/NU-1102**	Cyclohexene	Toluene	10
17	**Rh/NU-1102**	2-Cyclohexen-1-one	Toluene	25

Catalyst concentration: [a] 1 mol% Rh. [b] 0.1 mol% Rh.

Catalytic activity of Rh/MOFs

To check the activity of heterogeneous Rh/MOFs, hydrogenation of the model unsaturated hydrocarbons was performed. We selected 4 olefins: 1-octene, styrene, cyclohexene and 2-cyclohexen-1-one. All reactions were carried out in the presence of 1 mol% of rhodium in each catalyst and in toluene as the solvent, under mild reaction conditions at 30 °C and 1 atm of H_2 (balloon filled with H_2 gas). The comparison of the catalytic activities of **Rh/NU-1102** and **Rh/PCN-222** and **1c** is shown in Table 1. Both MOFs show a particularly good performance in the hydrogenation of 1-octene (99%, entries 6 and 13) and styrene (99%, entries 8 and 15). When the homogeneous molecular complex **1c** was used, after 24 hours of the reaction, the conversion of 1-octene and styrene was 46% and 14%, respectively. The difference in activity might be explained taking into consideration the rigid structure of MOFs, which does not allow for the aggregation of Rh moieties.[37] More significant difference in the activity of Rh/MOF catalysts can be observed in the hydrogenation of cyclohexene and 2-cyclohexen-1-one. For **Rh/PCN-222**, the yield of saturated hydrocarbons reached 99% after 24 h, and for **Rh/NU-1102**, lower yields for cyclohexene and 2-cyclohexen-1-one were recorded – 10% and 25%, respectively. We attributed this difference to topological differences between the two Rh/MOF networks.

To determine the catalytic activity of **Rh/PCN-222** with a higher loading of the substrate, hydrogenation of 1-octene was conducted with 0.1 mol% [Rh] at 30 °C and at 1 atm of H_2 (Fig. 4c). In this case, the conversion of 65% of 1-octene into octane was achieved after 24 h of the reaction, giving the turnover number (TON) and turnover frequency (TOF) of 650 and 0.451 s^{-1}, respectively.

To gain more insights into the catalytic activity of both systems, the kinetic profiles of the hydrogenation of 1-octene and styrene were determined. As shown in Fig. 4a, for both catalysts, almost 100% yield of the products was achieved after 10 hours of the reaction. Closer inspection of the kinetic curves suggests the presence of an induction period during the initial stage of the reaction course. After 4 hours, a sharp increase in conversion can be observed, which indicates that

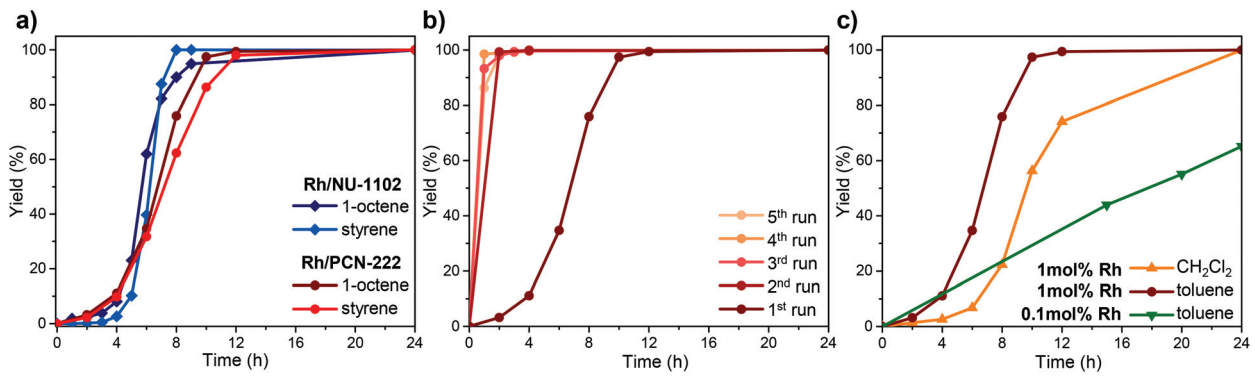

Fig. 4 (a) Comparison of the kinetic profiles of hydrogenation of selected unsaturated hydrocarbons by **Rh/NU-1102** and **Rh/PCN-222**; (b) recycling test (5 runs) of **Rh/PCN-222** in the hydrogenation of 1-octene; and (c) the effect of solvent and %mol of Rh in the hydrogenation of 1-octene by **Rh/PCN-222**.

the catalytic system requires an activation step to form an active species in the hydrogenation of olefins.[62] Next, the recycling tests were carried out to check whether the MOF-based catalyst remains active after the first catalytic cycle. The kinetic profiles for the hydrogenation of 1-octene by **Rh/PCN-222** during 5 consecutive runs are shown in Fig. 4b. To our pleasant surprise, the induction period was not observed in the second and all subsequent catalytic cycles. The conversion of 99% of 1-octene into octane was achieved after only 2 h of the reaction. The observed change in the activity of **Rh/PCN-222** indicates that the catalyst remains in its activated form after the first hydrogenation run. The integrity and structure of the catalyst after 5 consecutive runs was examined by the X-ray diffraction study. The PXRD patterns of **Rh/PCN-222** before and after the catalytic runs confirmed the preservation of the MOF structure (Fig. S44†). Moreover, the XPS analysis confirmed the unaltered Zr/Rh ratio in the **Rh/PCN-222** catalysts (see the ESI, section S4.2†). Furthermore, to verify if the reaction is truly heterogeneous and is not catalyzed by soluble rhodium complexes which could leach from the MOF, the ICP study was performed after the second cycle of the catalytic reaction. First, the catalyst was washed with toluene and then carefully dried under vacuum. Based on the ICP analysis for the Rh/MOF before and after the catalytic reaction, the Zr/Rh metal ratio was maintained.

The activities of **1c** and the Rh/MOFs were also compared in dichloromethane as the solvent. All catalysts were active; however, lower yields were obtained after 24 h of the reaction, in comparison with the reactions carried out in toluene (Table 1). Importantly, the major decrease in activity was observed for the molecular system **1c**. Examination of the kinetic curves (Fig. 4c) leads to a conclusion that the catalytic system tested in dichloromethane requires longer activation time than the analogous reaction in toluene.

Catalyst activation pathway studied by *in situ* DRIFTS

Carbon monoxide is a sensitive ligand to the coordination mode of the metal center. As we discussed above, carbonyl ligands in the Rh/MOFs are strongly attached to the rhodium centers. The presence of H_2 atmosphere, however, significantly changes this situation. To observe the transformations of CO ligands in the Rh/MOFs in the presence of H_2, an *in situ* DRIFTS solid state study was performed. DRIFTS spectra were measured at specific time intervals during the test, under H_2 flow at 30 °C.

From the measured spectra, we attempted to identify the active forms of the tested catalysts. Firstly, after the exposure of **Rh/PCN-222** to the H_2 atmosphere at 30 °C, a significant decrease in the intensity of the carbonyl bands at 2064 and 2006 cm^{-1} was observed during 90 minutes (Fig. 5c) of the experiment. The decrease in the intensity of the carbonyl bands is accompanied by the appearance of a new band at 1703 cm^{-1}, which indicates the formation of the formyl group Rh–CHO (Fig. 5d). Moreover, new bands also appear at 2936 cm^{1} and 2861 cm^{1}, characteristic of C–H vibrations in formic acid (Fig. 5a). In this case, the transformation of the

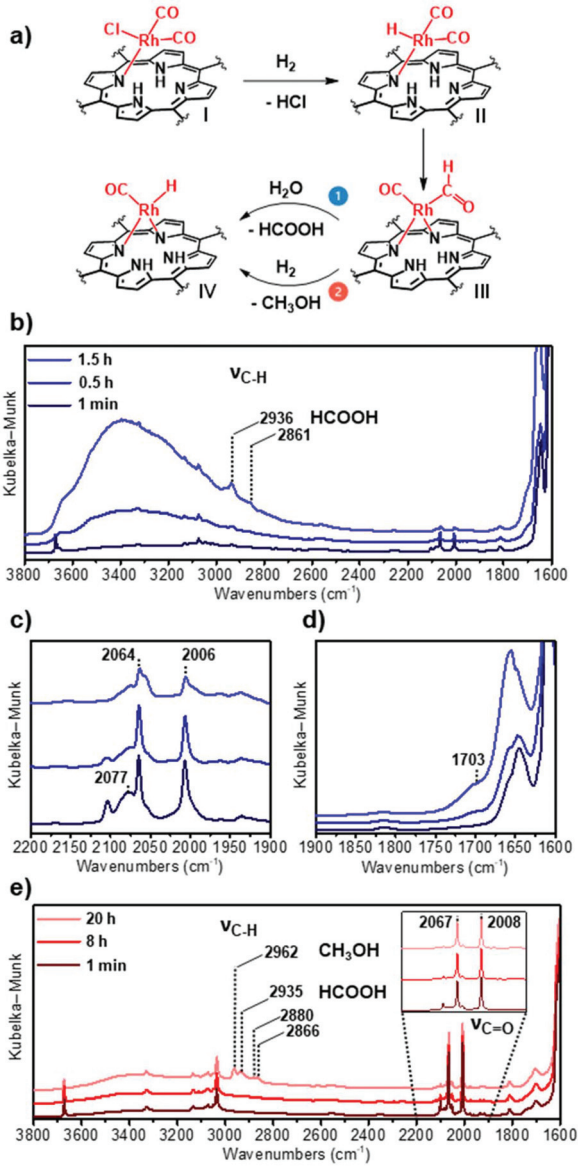

Fig. 5 (a) Proposed catalyst activation pathways for **Rh/PCN-222** (path 1) and **Rh/NU-1102** (path 2); comparison of the *in situ* DRIFTS spectra for the Rh/MOFs in the presence of H_2 at different time intervals for: **Rh/PCN-222** (b–d) and **Rh/NU-1102** (e).

CO ligand, in the presence of H_2 and H_2O, may lead to the formation of formic acid and Rh–H moieties (Fig. 5a). When the reaction was carried out at 120 °C, a significant decrease in the intensity of carbonyl bands was observed only after 5 min with the concomitant formation of HCOOH (Fig. S51†). To check whether moisture has an influence on the activation of **Rh/PCN-222**, the reaction with H_2 was monitored after drying the reaction chamber for 48 h at 100 °C. In this case, a much longer treatment of **Rh/PCN-222** with H_2 was required to observe the decrease of CO vibrations (Fig. S50†). We concluded that the presence of moisture accelerates the activation process of **Rh/PCN-222**, leading to formic acid as the final product (path 1, Fig. 5a). In contrast to **Rh/PCN-222**, after the

exposure of **Rh/NU-1102** to H_2 at 30 °C, only a slight decrease in the intensity of carbonyl bands at 2067 and 2008 cm^{-1} was observed (Fig. 5e).

Then, after the next 20 h, apart from the vibrations characteristic of HCOOH: 2935 cm^{-1}, 2880 cm^{-1} and 2866 cm^{-1}, another vibration at 2962 cm^{-1} was identified, which can be assigned to CH_3OH (Fig. 5e). This observation suggests a different activation pathway for **Rh/NU-1102** (path 2, Fig. 5a). The formation of CH_3OH is observed when water accessibility is lower and the reduction of carbonyl group with H_2 proceeds further. This change in the activity of **Rh/NU-1102** in comparison with **Rh/PCN-222** might be associated with different compositions and connectivities of zirconium nodes (12-connected *vs.* 8-connected node topology), and larger separation of Rh centers and Zr nodes. Because **Rh/PCN-222** has smaller pores, therefore guest molecules (*e.g.* water) can remain trapped in the porous MOF structure more efficiently and participate in the catalytic process.

Conclusions

In summary, we demonstrated a simple post-synthetic modification of porphyrin-based metal–organic frameworks with robust and easily accessible phosphine-free rhodium(I) precursor. The newly obtained Rh/MOFs proved to be efficient heterogeneous catalysts in the hydrogenation of unsaturated hydrocarbons under mild conditions. The kinetic study showed that Rh/MOFs require an activation step with molecular hydrogen yielding a catalytically active species. Based on the *in situ* DRIFTS study, a possible activation pathway is proposed with the generation of formic acid or methanol. This simple post-synthetic modification approach presents new possibilities for the utilization of Rh-based catalytic systems with robust porphyrin-based MOFs as supports.

Author contributions

A. M. S. carried out the synthesis, most of the characterization studies of the materials and the catalytic study, M. J. synthesized compounds **2a** and **2b**, M. S. carried out the single-crystal X-ray diffraction measurements and solved the crystal structures, and W. T. carried out the XPS analysis. A. M. S. and W. B. analysed the experimental data and wrote the manuscript, and W. B. and A. M. T. supervised the project.

Conflicts of interest

There are no conflicts to declare.

Acknowledgements

The authors would like to thank the National Science Centre, Poland: UMO-2014/14/E/ST5/00652 (A. M. S. and W. B.) and UMO-2017/25/B/ST5/00394 (A. M. T.), for its support towards this research. XPS research was funded by a statutory activity subsidy from the Polish Ministry of National Education for the Faculty of Chemistry of Wrocław University of Science and Technology.

Notes and references

1 B. Richter, A. L. Spek, G. van Koten and B.-J. Deelman, *J. Am. Chem. Soc.*, 2000, **122**, 3945–3951.
2 J. Daubignard, M. Lutz, R. J. Detz, B. de Bruin and J. N. H. Reek, *ACS Catal.*, 2019, **9**, 7535–7547.
3 K. Tanaka, *Rhodium Catalysis in Organic Synthesis: Methods and Reactions*, John Wiley & Sons, 2019.
4 P. Etayo and A. Vidal-Ferran, *Chem. Soc. Rev.*, 2012, **42**, 728–754.
5 P. W. N. M. van Leeuwen and C. Claver, *Rhodium Catalyzed Hydroformylation*, Springer Science & Business Media, 2002.
6 R. Franke, D. Selent and A. Börner, *Chem. Rev.*, 2012, **112**, 5675–5732.
7 A. Börner and R. Franke, *Hydroformylation: Fundamentals, Processes, and Applications in Organic Synthesis*, Wiley-VCH GmbH & Company KGaA, 2016.
8 P. W. N. M. van Leeuwen, *Homogeneous Catalysis: Understanding the Art*, Kluwer Acad. Publ, Dordrecht, 2004.
9 M. Beller, *Catalytic Carbonylation Reactions*, Springer Science & Business Media, 2006.
10 P. Kalck, C. Le Berre and P. Serp, *Coord. Chem. Rev.*, 2020, **402**, 213078.
11 A. Behr and P. Neubert, *Applied Homogeneous Catalysis*, John Wiley & Sons, 2012.
12 J. Lee, O. K. Farha, J. Roberts, K. A. Scheidt, S. T. Nguyen and J. T. Hupp, *Chem. Soc. Rev.*, 2009, **38**, 1450–1459.
13 Y.-S. Wei, M. Zhang, R. Zou and Q. Xu, *Chem. Rev.*, 2020, **120**, 12089–12174.
14 Z. Chen, J. Chen and Y. Li, *Chin. J. Catal.*, 2017, **38**, 1108–1126.
15 A. E. Platero-Prats, M. Iglesias, N. Snejko, Á. Monge and E. Gutiérrez-Puebla, *Cryst. Growth Des.*, 2011, **11**, 1750–1758.
16 O. Kozachuk, I. Luz, F. X. Llabrés i Xamena, H. Noei, M. Kauer, H. B. Albada, E. D. Bloch, B. Marler, Y. Wang, M. Muhler and R. A. Fischer, *Angew. Chem., Int. Ed.*, 2014, **53**, 7058–7062.
17 R. A. Peralta, M. T. Huxley, J. D. Evans, T. Fallon, H. Cao, M. He, X. S. Zhao, S. Agnoli, C. J. Sumby and C. J. Doonan, *J. Am. Chem. Soc.*, 2020, **142**, 13533–13543.
18 Q. Yang, Q. Xu, S.-H. Yu and H.-L. Jiang, *Angew. Chem., Int. Ed.*, 2016, **55**, 3685–3689.
19 P. Wang, J. Zhao, X. Li, Y. Yang, Q. Yang and C. Li, *Chem. Commun.*, 2013, **49**, 3330–3332.
20 G. Lu, S. Li, Z. Guo, O. K. Farha, B. G. Hauser, X. Qi, Y. Wang, X. Wang, S. Han, X. Liu, J. S. DuChene, H. Zhang,

Q. Zhang, X. Chen, J. Ma, S. C. J. Loo, W. D. Wei, Y. Yang, J. T. Hupp and F. Huo, *Nat. Chem.*, 2012, **4**, 310–316.
21 Y. Yang, F. Wang, Q. Yang, Y. Hu, H. Yan, Y.-Z. Chen, H. Liu, G. Zhang, J. Lu, H.-L. Jiang and H. Xu, *ACS Appl. Mater. Interfaces*, 2014, **6**, 18163–18171.
22 J. Zhuang, L.-Y. Chou, B. T. Sneed, Y. Cao, P. Hu, L. Feng and C.-K. Tsung, *Small*, 2015, **11**, 5551–5555.
23 W. R. Heinz, T. Kratky, M. Drees, A. Wimmer, O. Tomanec, S. Günther, M. Schuster and R. A. Fischer, *Dalton Trans.*, 2019, **48**, 12031–12039.
24 V. Bernales, D. Yang, J. Yu, G. Gümüşlü, C. J. Cramer, B. C. Gates and L. Gagliardi, *ACS Appl. Mater. Interfaces*, 2017, **9**, 33511–33520.
25 D. T. Genna, A. G. Wong-Foy, A. J. Matzger and M. S. Sanford, *J. Am. Chem. Soc.*, 2013, **135**, 10586–10589.
26 D. T. Genna, L. Y. Pfund, D. C. Samblanet, A. G. Wong-Foy, A. J. Matzger and M. S. Sanford, *ACS Catal.*, 2016, **6**, 3569–3574.
27 W. M. Bloch, A. Burgun, C. J. Coghlan, R. Lee, M. L. Coote, C. J. Doonan and C. J. Sumby, *Nat. Chem.*, 2014, **6**, 906–912.
28 A. Burgun, C. J. Coghlan, D. M. Huang, W. Chen, S. Horike, S. Kitagawa, J. F. Alvino, G. F. Metha, C. J. Sumby and C. J. Doonan, *Angew. Chem., Int. Ed.*, 2017, **56**, 8412–8416.
29 Y. Benseghir, A. Lemarchand, M. Duguet, P. Mialane, M. Gomez-Mingot, C. Roch-Marchal, T. Pino, M.-H. Ha-Thi, M. Haouas, M. Fontecave, A. Dolbecq, C. Sassoye and C. Mellot-Draznieks, *J. Am. Chem. Soc.*, 2020, **142**, 9428–9438.
30 A. A. Kassie, P. Duan, E. T. McClure, K. Schmidt-Rohr, P. M. Woodward and C. R. Wade, *Inorg. Chem.*, 2019, **58**, 3227–3236.
31 L. Feng, K.-Y. Wang, E. Joseph and H.-C. Zhou, *Trends Chem.*, 2020, **2**, 555–568.
32 S. J. Thompson, M. R. Brennan, S. Y. Lee and G. Dong, *Chem. Soc. Rev.*, 2018, **47**, 929–981.
33 C. Duchemin and N. Cramer, *Chem. Sci.*, 2019, **10**, 2773–2777.
34 E. J. T. Phipps and T. Rovis, *J. Am. Chem. Soc.*, 2019, **141**, 6807–6811.
35 H.-Y. Thu, G. S.-M. Tong, J.-S. Huang, S. L.-F. Chan, Q.-H. Deng and C.-M. Che, *Angew. Chem., Int. Ed.*, 2008, **47**, 9747–9751.
36 Y. Qiu, A. Scheremetjew and L. Ackermann, *J. Am. Chem. Soc.*, 2019, **141**, 2731–2738.
37 G. H. Imler, M. J. Zdilla and B. B. Wayland, *J. Am. Chem. Soc.*, 2014, **136**, 5856–5859.
38 E. A. Boyd, D. Lionetti, W. C. Henke, V. W. Day and J. D. Blakemore, *Inorg. Chem.*, 2019, **58**, 3606–3615.
39 P. Jurt, O. G. Salnikov, T. L. Gianetti, N. V. Chukanov, M. G. Baker, G. L. Corre, J. E. Borger, R. Verel, S. Gauthier, O. Fuhr, K. V. Kovtunov, A. Fedorov, D. Fenske, I. V. Koptyug and H. Grützmacher, *Chem. Sci.*, 2019, **10**, 7937–7945.
40 S. Kim, F. Loose, M. J. Bezdek, X. Wang and P. J. Chirik, *J. Am. Chem. Soc.*, 2019, **141**, 17900–17908.
41 B. R. James and D. V. Stynes, *J. Am. Chem. Soc.*, 1972, **94**, 6225–6226.
42 H. W. Bosch and B. B. Wayland, *J. Chem. Soc., Chem. Commun.*, 1986, 900–901.
43 J. P. Collman, Y. Ha, R. Guilard and M. A. Lopez, *Inorg. Chem.*, 1993, **32**, 1788–1794.
44 X. Fu and B. B. Wayland, *J. Am. Chem. Soc.*, 2004, **126**, 2623–2631.
45 C. Stangel, G. Charalambidis, V. Varda, A. G. Coutsolelos and I. D. Kostas, *Eur. J. Inorg. Chem.*, 2011, **2011**, 4709–4716.
46 M. H. Beyzavi, N. A. Vermeulen, A. J. Howarth, S. Tussupbayev, A. B. League, N. M. Schweitzer, J. R. Gallagher, A. E. Platero-Prats, N. Hafezi, A. A. Sarjeant, J. T. Miller, K. W. Chapman, J. F. Stoddart, C. J. Cramer, J. T. Hupp and O. K. Farha, *J. Am. Chem. Soc.*, 2015, **137**, 13624–13631.
47 D. Feng, Z.-Y. Gu, J.-R. Li, H.-L. Jiang, Z. Wei and H.-C. Zhou, *Angew. Chem., Int. Ed.*, 2012, **51**, 10307–10310.
48 T. C. Wang, W. Bury, D. A. Gómez-Gualdrón, N. A. Vermeulen, J. E. Mondloch, P. Deria, K. Zhang, P. Z. Moghadam, A. A. Sarjeant, R. Q. Snurr, J. F. Stoddart, J. T. Hupp and O. K. Farha, *J. Am. Chem. Soc.*, 2015, **137**, 3585–3591.
49 A. M. Abeysekera, R. Grigg, J. Trocha-Grimshaw and V. Viswanatha, *J. Chem. Soc., Perkin Trans. 1*, 1977, 36–44.
50 A. Srinivasan, M. Toganoh, T. Niino, A. Osuka and H. Furuta, *Inorg. Chem.*, 2008, **47**, 11305–11313.
51 A. Srinivasan, H. Furuta and A. Osuka, *Chem. Commun.*, 2001, 1666–1667.
52 S. Sarkar, S. Li and B. B. Wayland, *Inorg. Chem.*, 2011, **50**, 3313–3319.
53 G. H. Imler, M. J. Zdilla and B. B. Wayland, *Inorg. Chem.*, 2013, **52**, 11509–11513.
54 A. M. Abeysekera, R. Grigg, J. Trocha-Grimshaw and V. Viswanatha, *J. Chem. Soc., Perkin Trans. 1*, 1977, 36–44.
55 E. Teuma, M. Loy, C. Le Berre, M. Etienne, J.-C. Daran and P. Kalck, *Organometallics*, 2003, **22**, 5261–5267.
56 S. Yamazaki, M. Yao, M. Asahi, H. Sato, A. Yamano and T. Ioroi, *Dalton Trans.*, 2015, **44**, 13823–13827.
57 X. Xue, J. Yu, Y. Han, X. Xiao, Z. Shi, H. Mao and D. Mao, *J. Ind. Eng. Chem.*, 2020, **86**, 220–231.
58 Z. Ren, Y. Liu, Y. Lyu, X. Song, C. Zheng, S. Feng, Z. Jiang and Y. Ding, *J. Catal.*, 2019, **369**, 249–256.
59 The reason for these discrepancies is a strong dependence of the electron binding energy of the different valence states on the coordination environment of rhodium.
60 We observed that the "aging process" in the crystals occurs spontaneously over time. In general, Rh(I) species are very reactive and can be oxidized to Rh(III) under ambient conditions. The X-ray diffraction studies were performed on "aged" samples **Rh/PCN-222(a)** and **Rh/NU-1102(a)**.
61 Assuming that the metal oxides ZrO_2 and Rh_2O_3 are the decomposition products.
62 The observed induction period can be significantly reduced in the presence of water. See section S5.5 in the ESI.†

